EMG-based Human-In-The Loop Bayesian Optimization to Assist Free Leg Swinging

Salvador Echeveste, Pranav A. Bhounsule

***Abstract*—Manual tuning of exoskeleton control parameters is tedious and often ineffective at tuning control laws for multiple subjects. One of the ways to circumvent this issue is the use of Human-In-The-Loop (HIL) optimization, which automatically identifies well-performing parameters. Currently, most HIL optimization methods rely on metabolic cost, which requires a substantial amount of data to reach a steady state, often requiring at least a minute of data to estimate. Surface electromyography signals (EMG) have emerged as a promising alternative physiological metric in the world of HIL optimization. EMG data is more convenient to collect and significantly faster to acquire. The focus of this work is to develop a faster EMG-based optimization method to tune free leg-swinging assistance controllers which can be adapted to several exoskeleton-targeted activities. The method can tune controllers in as little as 15 seconds per condition or 2.38 ± 0.4 min of total optimization. The resultant optimal controller can outperform baselines with average muscle activity reductions of 16.1% against no device, 21.7% against zero torque, and 15.1% against a general controller. This establishes the efficiency and effectiveness of tuning with EMG-based HIL optimization.**

***Index Terms*—exoskeletons, human-in-the-loop, electromyography, and hyperparameter optimization.**

I. Introduction

DESPITE several examples of moderate energy reduction improvements in the realm of assistive exoskeletons, most devices still cannot fully account for high inter-subject variability in physiological responses [1–7]. Slight differences in exoskeleton actuation can significantly affect how users benefit from the assistance. Therefore, more thorough individualized control tuning can achieve better assistance to reduce the effort required to perform certain activities such as walking [8–14]. The ever-increasing demand for wearable robotics has made manual tuning of control parameters for each individual time-consuming and often strenuous [11, 15–17]. With human-in-the-loop (HIL) technology, a paradigm that eliminates the need for expert intervention and extensive research hours, optimal parameters can be automatically identified and tuned in real-time via physiological signals [8, 11, 14, 18].

While several HIL optimization methods have shown success [2, 8, 17–19], they commonly rely on metabolic cost—a measure with a prolonged acquisition time [20–23]. Data measurements for metabolic cost often adapt slowly [12], estimations require substantial historical data [24], and signal readings are influenced by complex neurocognitive factors [22]. Due to these factors, traditional metabolic cost calculations may require 4-6 minutes of data per condition. Some alternatives have explored accelerating this process by estimating metabolic cost steady state. However, metabolic cost estimations typically demand one to two minutes of data per evaluation [20]. Since thorough optimization requires the evaluation of several conditions, the acquisition time aggregates to a lengthy procedure, allowing the user preference to shift before optimization completion [8, 14]. A faster promising alternative is surface electromyography (EMG), a non-invasive measure of muscle activity voltage.

The integration of EMG and exoskeletons is not a novel concept; EMG signal input has been used for modulating control in exoskeletons for several decades [23, 25]. While most implementations have focused on volitional control of upper body prosthetics and orthotics, some devices employ EMG-control to assist the lower body [26]. Studies even demonstrate the successful use of EMG signals to optimally tune walking exoskeleton controllers [8, 17]. However, utilizing EMG as an objective for HIL optimization remains underexplored, likely due to inherent issues such as signal noise, poor repeatability, and the potential for procedural complexity [27, 28]. Despite these drawbacks, EMG offers a shorter acquisition time, greater convenience to researchers, lower discomfort for subjects, and the ability to reflect reductions in energy economy effectively [27, 29–31]. Therefore, properly harnessing this physiological metric has the potential to significantly reduce the time required for current hardware optimization methods.

Our focus centers on stationary leg-swinging assistance due to its more stable, unilateral nature. Leg swinging is a pivotal component of walking and the hip is a natural contender as the joint to target, given its crucial contribution of up to 45% of the mechanical power during the walking gait cycle [1, 32]. Several hip-targeted exoskeletons have shown moderate success in reducing metabolic cost, making them ideal candidates for a more thorough controller tuning process using EMG-based HIL optimization [1, 33].

In addition to using EMG as the cost function, we employ Bayesian optimization to improve the sample efficiency of our HIL optimization approach. We select Bayesian optimization for its noise tolerance, ability to quickly optimize physiological signals, and documented history of successful outcomes in HIL optimization [18, 31, 34].

This work delves into the parameter optimization of an autonomous, self-contained, semi-rigid hip exoskeleton with one degree of freedom (hip extension, hip flexion) to assist leg swinging at two different swing frequencies. The overview of our methods is highlighted by (Fig. 1). The novel contributions of this work are the following: 1) We establish a reliable, time-efficient EMG-based HIL optimization process capable of tuning assistance controllers. 2) The proposed method is capable of tuning faster than metabolic cost approaches and other established EMG-based HIL optimization methods.

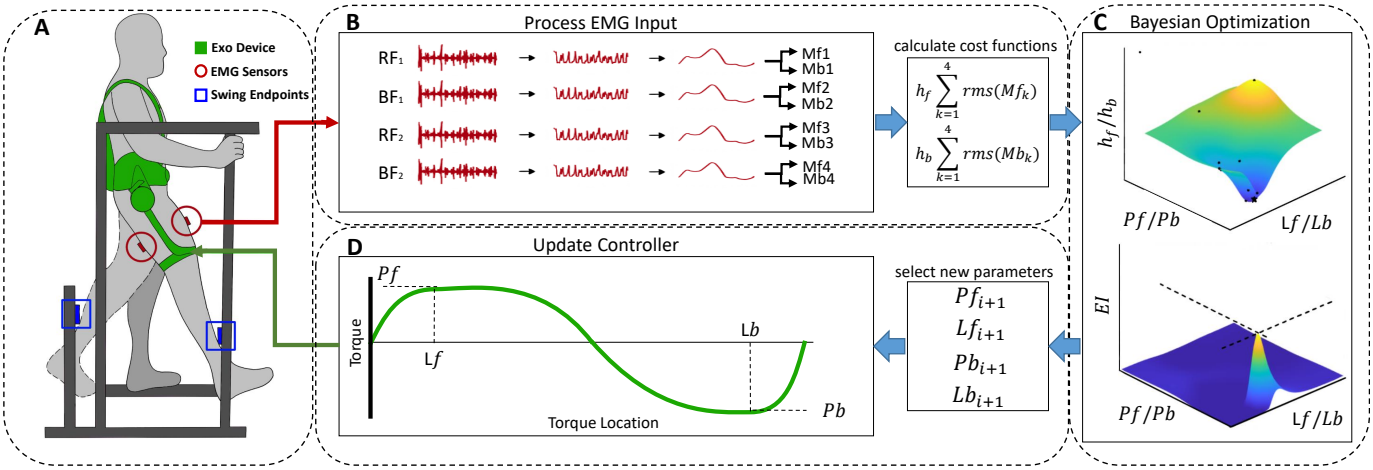

Fig. 1. Overview of EMG-HIL Bayesian Optimization A) Visualization of the swinging setup where the device, sensors, and structure are shown and labeled. B) The EMG data processing pipeline of the four signals used. Further details in Fig.3. C) An overview of the optimization process using Bayesian optimization to tune four parameters using two cost functions. D) Controller details including how the parameters shape the profile.

3) We tune controllers to effectively assist stationary leg swinging with notable statistically significant reductions in EMG activity.

II. Methods

A. Experimental Setup

1) Hip Exoskeleton Device: The device used in this study is a custom hip exoskeleton intended to assist hip flexion and extension. The device is composed of a 24V Brushless DC (BLDC) motor (AK70-10 T motor, 25Nm peak torque, 8Nm nominal torque), attached by a series of straps (shoulder straps, leg straps,belt) and limited rigid components (plastic braces, aluminum links). The actuation is provided in a quasi-direct manner with an open-loop torque controller that allows back-driveability. The angle of the hip is measured by an inertial measurement unit (IMU) (Adafruit BNO055, close-loop triaxial 16-bit gyroscope, 100 Hz reading frequency). The device allows for a range of motion between -30°(extension/posterior) and 90 °(flexion/anterior). The hip exoskeleton also contains elements to prevent injury and discomfort. These features include hard stops at the end of the range of motion to prevent over-extension beyond the comfortable range of motion of the human anatomy, two emergency stop buttons (one to stop the torque and the other to shut down the device), and integrated safety checks in the code to ensure the torque magnitude does not exceed 25 Nm.

All control is done in Python 3.9.2 onboard a Raspberry Pi 4. The controller is designed to mimic several torque shapes that are found capable of assisting effectively in a previous study [35]. The shape of the controller is defined using a set of cubic Bezier curves relating torque magnitude to angle. The Bezier curves are constructed using four points in a two-dimensional plane across the swing phase (Fig.2 B). Each of these points is defined with a location and magnitude coordinate, therefore a total of eight inputs. The use of Bezier curves allows the torque profile to take on more versatile shapes without explicit analytic definition. For the activity of this study, the number of control inputs is further reduced by setting the location of the control points to be 5°apart and setting the magnitudes of both to be equal. Therefore, it is only necessary to specify the location (L), and magnitude (P) of one point per direction. This reduces the number of inputs from eight to four. This type of controller demonstrated a promising assistance profile in the pilot study and in previous work [35]. Control of the leg swing is split into two different directions, forward swing and backward swing. On a high level, the controller can target each of these states separately using a finite state machine (FSM), where the transitions are triggered by the change in the direction of angular velocity measured by the IMU. The controller aligns torque direction with velocity direction to exclusively supply positive work assistance to not inhibit natural swing dynamics.

2) Bayesian Optimization: Bayesian optimization serves as a robust method to identify the optimal set of parameters when the objective function is noisy and expensive to evaluate. The approach entails constructing a probabilistic surrogate model of the objective function based on posterior data that incorporates a prior distribution. By leveraging this model to predict outcomes for different parameter settings, it can select the next parameter setting to evaluate through an acquisition function that uses a strategic trade-off between exploration (trying new settings) and exploitation (utilizing the best-known settings) [34].

In this study, the probabilistic model adopted is a Gaussian process (GP), assuming the prior distribution of the objective function is a realization of a GP with added Gaussian noise (Eq. 1). The GP is characterized by a mean function, $m(x)$, and a covariance function, $k(x, x')$. Both functions are estimated based on a set of initialization data.

$$f(x) \sim GP(m(x), k(x, x^{'})) \tag{1}$$

The covariance function is an Automatic Relevance Determination (ARD) squared exponential kernel (Eq. 2), where, σ_f^2 is the signal variance of the estimated cost variance, and l is the length scale parameter.

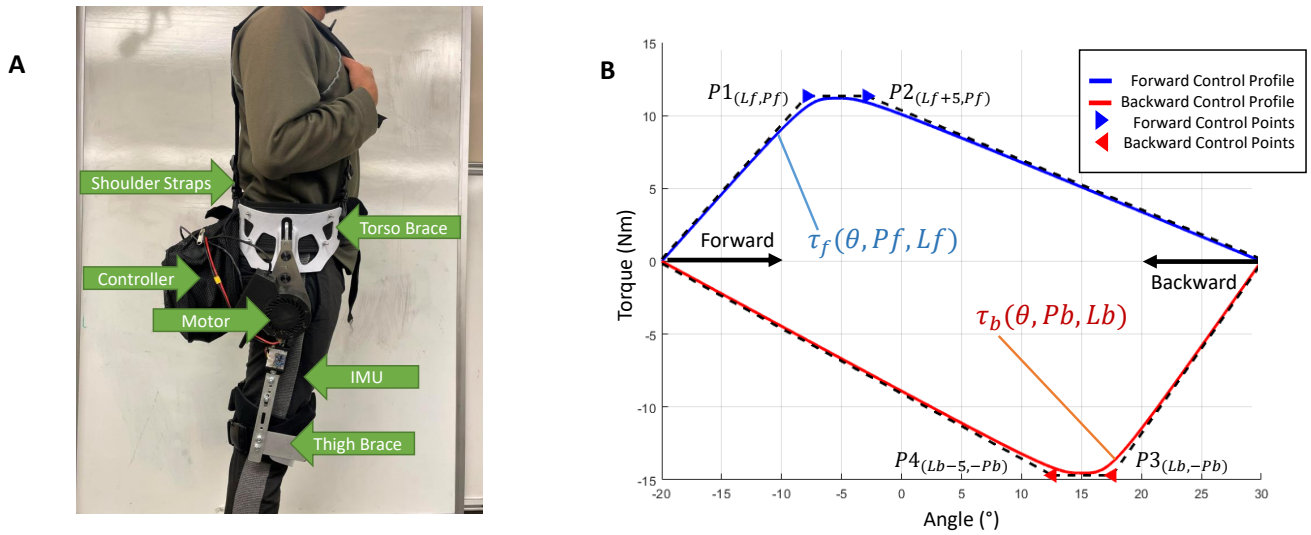

Fig. 2. A) An illustration of the exoskeleton device detailing all the main components. B) An overview of the controller constructs a relationship between torque and angle using segmented Bezier curves. The location of the four control points. Control points P1 and P2 are dependent on P_f and L_f while P3 and P4 are dependent on P_b and L_b. The torque functions for forward and backward actuation are represented as τ_f and τ_b respectively.

$$k(x, x^{'}) = \sigma_f^2 e^{-\frac{(x-x^{'})^2}{2l^2}} \tag{2}$$

The acquisition function employed in the optimization process is the Expected Improvement (EI) function. This function quantifies the expected improvement in the objective function over the best-known value. The next parameter set to evaluate is determined by maximizing the EI function (Eq. 5), where f_{best} is the best-known value of the objective function, and the expectation is taken over the posterior distribution of the GP.

$$EI(x) = E[\max(f(x^{'}) - f_{best}, 0)] \tag{3}$$

The determination of the next sample parameter set follows the maximization of the EI function:

$$x_{n+1} = \text{argmax}(EI\,[x_*]) \tag{4}$$

where the $argmax$ function returns the parameter set which maximizes the EI in the parameter matrix, x_*.

B. EMG Data

1) Sensor Data Processing: EMG sensors (Trigno, Delsys, MA, USA) are placed on the subject's legs. Surface EMG data is collected from the rectus femoris (RF) and bicep femoris (BP) of each leg at a frequency of 1778 Hz. Angle orientation data is collected from the same sensor at a frequency of 148Hz. Each of the four sensors is placed on the respective muscle by following Surface Electromyography for the Non-Invasive Assessment of Muscles (SENIAM) instructions [36]. SENIAM provides standardized methods for electrode placement to ensure consistency and comparability. Once all sensors are placed, a maximum voluntary contraction (MVC) of each muscle targeted is measured by asking the participant to exert their muscle as much as possible in a safe manner. The MVC values are recorded to be later used for EMG normalization.

The sensor data from the four EMG sensors is processed in MATLAB. The pipeline developed was found to produce the best signal-to-noise ratio in a pilot study and is illustrated in Fig. 3. The first step is for each EMG signal to be put through a bandpass with a high pass of 20Hz and a low pass of 450 Hz followed by an outlier detection algorithm that replaces extreme values that are further than three standard deviations from the mean using modified Akima cubic Hermite interpolation [37] (Fig. 3 A). The EMG values are then rectified by taking the absolute value of the signal and subtracting the mean of the non-rectified values to account for the DC offset (Fig. 3 B). Once rectified, the signal is smoothed using a three-filter process (Fig. 3 C). The first filter applied is a moving max filter with a max window size of 50 data points (less than 0.25% of the total data set length). Next, a small discretization filter is applied to reduce the resolution of the data using bin sizes between 10 and 30. The last filter used is a moving average filter with a maximum window size of up to 400 data points ($\sim$1.6% of total data length). After smoothing, the data is normalized by dividing the signal by each sensor's respective MVC value allowing the four signals to be combinable (Fig. 3 D). Now the angle data is linearly interpolated to match the frequency of the EMG data and then differentiated with respect to time. Velocity data is used to split the EMG data into forward and backward data sets (Fig. 3 E). Both EMG data sets are now epoched and averaged into a single swing representation (Fig. 3 F). This process produces eight separate representations of the EMG data. Two cost functions, one for forward swing and one for backward swing, are calculated from these eight models by summing the root mean squared of the models in the same direction. The equation for the cost functions can be found in Eq. 5, where $h^{i=f}$ represents a forward cost function, $h^{i=b}$ represents the

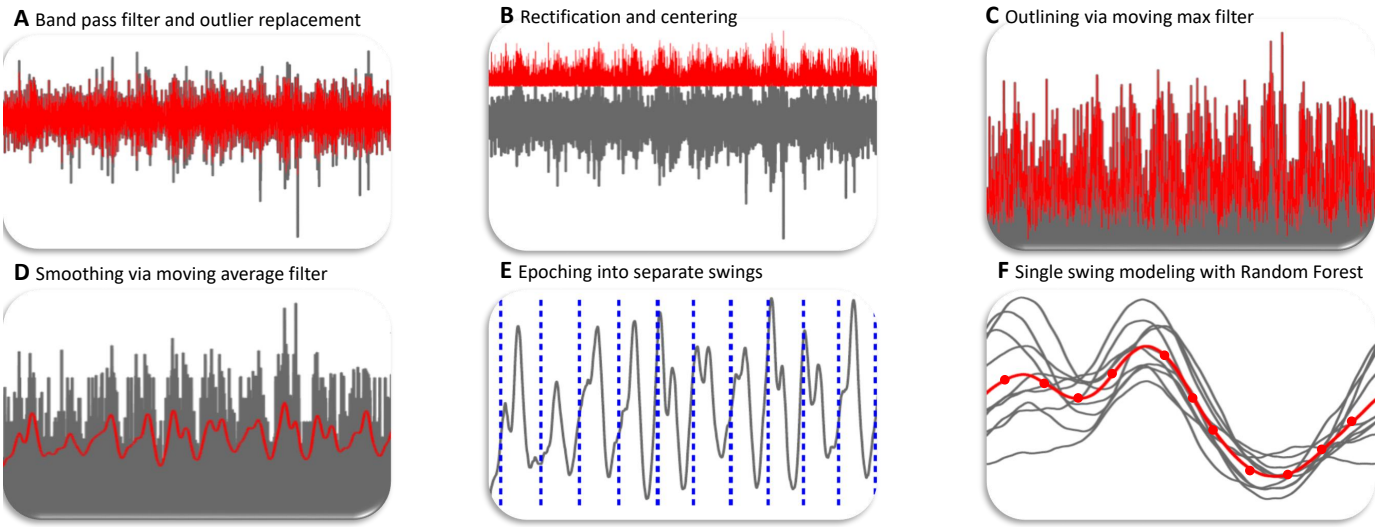

Fig. 3. Signal processing includes A) a bandpass filter with a high pass of 20Hz and a low pass of 450 Hz plus an outlier replacement of extreme values beyond 3 standard deviations using a modified Akima cubic Hermite interpolation; B) rectification by taking the absolute value and subtracting the mean value of the previous signal; C) a moving max and discretization filter to outline the shape of the signal; D) a moving average filter to smooth noise followed by normalization against the MVC value for each sensor; E) partitioning the data into separate swings; F) and a data aggregation process using an averaged representation of the epochs produces a single output represention. Red indicates the signal after the current process, while gray indicates the signal before the process.

backward cost function.

$$h^i = \sum_{n=1}^{4} \text{rms}(M_n^f) \tag{5}$$

The EMG data from the muscle models for the rectus femoris and bicep femoris of the swing leg, and the rectus femoris and the bicep femoris of the stance leg are represented as $M_1^d, M_2^d, M_3^d, M_4^d$ respectively. The variable f is used to represent forward swing data while b represents backward swing data. This is done for both slow-swing data sets and fast-swing data sets.

2) Data Convergence: To ensure the reliability of data collected within a relatively short acquisition time, it's crucial to confirm its sufficiency and consistency. This involves identifying when the electromyography (EMG) data reaches a steady state.To accomplish this, a mathematical approach is employed.

First, the EMG data from all four signals are consolidated into a single matrix, denoted as E. Then, a running average is computed for each column of this matrix using Equation 6. Subsequently, the rate of change (R) of these running averages with respect to time is determined through differentiation. These rates of change are aggregated into a single vector, g, using Equation 7.

$$R(i) = \frac{1}{i} \sum_{i=1}^{i} E_i \tag{6}$$

$$g(i) = \sum_{j=1}^{4} \frac{dR_j(i)}{dt} \tag{7}$$

Next, statistical analysis is applied to this vector to discern when the combined rate of change of the EMG signals no longer significantly differs from zero, indicating a steady state. This is achieved by segmenting the vector into windows using a buffer method as described in Equation 8, with window size determined based on convergence frequency of 2Hz.

$$B(k,w) = \begin{bmatrix} g_1 & g_2 & \cdots & g_w \\ g_{w+1} & g_{w+2} & \cdots & v_{2w} \\ \vdots & \vdots & \ddots & \vdots \\ g_{n-w+1} & g_{n-w+2} & \cdots & g_n \end{bmatrix} \tag{8}$$

Within each window, a z-test is conducted, comparing the mean rate of change in the current window (k) with that of the previous window ($k-1$) (Equation 9). A p-value greater than 0.05 (using a significance level of 0.95) is sought to support the null hypothesis, indicating no significant difference between the means.

$$H_0 : \mu(B(k) - B(k-1)) = 0 \tag{9}$$

Additionally, a correlation analysis is performed at each window to assess the linear relationship between the current and previous windows, computed using the Pearson coefficient (Equation 10).

$$C(k) = corr(B(k), B(k-1)) \tag{10}$$

The combination of these methods determines the convergence point of the signal. Specifically, the steady-state time is identified as the point after which both the p-value exceeds 0.95 and the correlation coefficient reaches its maximum positive value. The final time stamp of the window meeting these criteria is designated as the steady-state time (Equation 11).

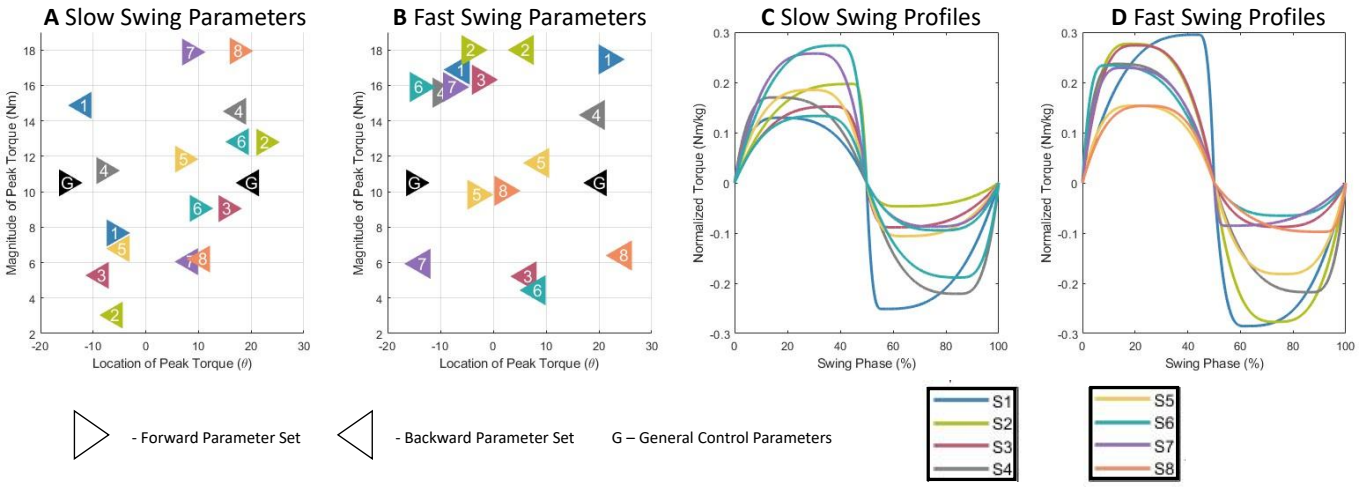

Fig. 4. This figure presents a comprehensive view of the swing controller concerning both controller parameters and torque profiles. A,B) Plots displaying the spatial distribution of controller parameters during the slow swing and fast swing. The x-axis represents the location, and the y-axis denotes the magnitude. C,D) showcasing the torque profile for the slow and fast swing, with the x-axis indicating the swing phase as a percentage, and the y-axis representing the normalized torque.

$$t_{steady-state} = max\left(i \| p > .05 \cap max(C)\right) \tag{11}$$

C. Experimental Protocol

The study is approved by the University of Illinois at Chicago Institutional Review Board (STUDY 1022-2022). A one-day protocol is conducted with eight healthy participants (age: 26.3 $\pm$ 3.2 years; weight: 64.6 $\pm$ 3.47 kg; height: 165.33 $\pm$ 11.13 cm, male: 5, female: 3). Subjects are asked to swing their right leg assisted and unassisted while their upper torso is supported by a custom rigid structure. The structure restricts the leg swing within a desired angle range (-20°to 30°from the vertical) using bumpers. Two swing frequencies, corresponding with normal walking frequencies [38], are tested (0. 67 Hz and 0.83 Hz). These frequencies are encouraged via the use of a metronome which provides the audible cue at which to make contact with each bumper. Participants are instructed to swing their leg at the beat of the metronome such that they make gentle contact with each bumper at each beat (Fig. 1 A). To account for two contacts per swing, the metronome is played at twice the desired swing frequency. A work-to-rest ratio of 1:2 is kept consistent throughout the experiment to reduce the effects of fatigue.

The three-hour experiment consists of four main sections: acclimation, parameter optimization, and validation.

1) Acclimation: During the acclimation section, subjects are exposed to nine different parameter sets for each swing frequency. The parameter sets are selected using a Latin hypercube sampling (LHS) to provide an even distribution of the parameter space. Each parameter set is supplied for 30-second trials in clusters of three before allowing rest. This results in three slow-frequency clusters and three fast-frequency clusters, each followed by a rest period of 90 seconds. The main focus of this section is to allow participants to learn how to interact with the assistance provided by the device before tuning.

2) HIL Optimization: The human-in-the-loop Bayesian optimization procedure involves a maximum of 12 trials for each swing frequency, each lasting 15 seconds. The selection of the maximum number of trials is based on observed convergence during the pilot test. To streamline the process, both swing frequencies are optimized concurrently within the same run, with the slower frequency sampled first, followed by a 10-second rest period, and then the faster frequency.

The initial four trials serve as initialization trials, allowing for sampling of the parameter space before the Bayesian optimization begins to select new parameter sets using the acquisition function. This optimization is conducted for up to eight trials to tune the two parameters for the forward and backward swing controllers in parallel, resulting in a total of two controllers with two phases each (four parameters per controller) being tuned synchronously. These controllers consist of a slow frequency controller with its forward and backward phases, and a fast frequency controller with its forward and backward phases.

Convergence is achieved when the same parameter set produces the best-performing controller three times within an allowable variation of $\pm$ 10%. All eight parameter sets must converge before the optimization is stopped. If this condition is not met, the experiment continues until the maximum number of search iterations is reached. The optimal controller is determined as the best-performing parameter set estimated by the Bayesian algorithm.

3) Validation: Following the identification of the optimal parameter set, its performance is evaluated against three baselines:

- No exoskeleton (NE), where the subject performs free swinging.
- Zero actuation (ZA), where the subject wears the device but it remains unpowered.
- General control (GC), where the subject receives assistance from a predefined intuition controller

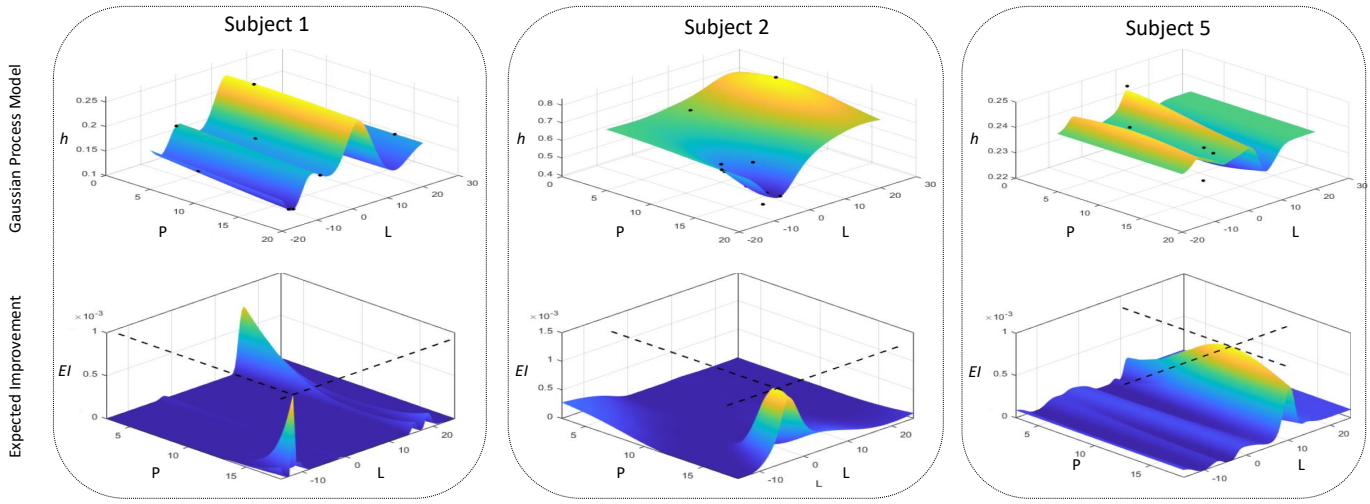

Fig. 5. Three samples of the surrogate and acquisition function optimization landscapes from Bayesian. The h variable represents the cost function, P and L are the two parameters tuned, and EI is the expected improvement for each parameter set. Lower values are favorable for the Gaussian process model and higher values are favorable for the expected improvement function.

supplying a magnitude of torque equivalent to the mean of the possible torque values at the beginning of each half swing.

The performance of the optimal and baseline conditions for each swing frequency is tested three times. During each iteration, a performance metric equivalent to the cost function, Eq.5, is calculated. Each condition is represented by a single mean value derived from the three observations. The percent change between the optimal mean (μ_{optimal}) and the mean of each baseline (μ_{baseline}) is then calculated. (Eq. 12).

$$\% \ \Delta = \left(\frac{\mu_{optimal} - \mu_{baseline}}{\mu_{baseline}} \right) \tag{12}$$

Data collection and processing for each trial follow the same protocol as the tuning trials. Any outliers in the data are identified and replaced with the center value of the data if they deviate by more than three standard deviations from the mean.

Statistical analysis between two conditions is paired. Since the data from most conditions are not normally distributed (Shapiro-Wilk test, $p < .05$), a non-parametric Wilcoxon test is used to assess the statistical significance of the comparison[39]. The null hypothesis assumes that the average percent change between the optimal and a particular baseline is zero, with a significance level of $p < .05$.

Additionally, each subject's perceived effort is rated according to Borg's scale, which exhibits a significant positive correlation with heart rate, providing supplementary insights into the subjective experience of the experimental conditions.

III. Results

One critical aspect to verify when working with EMG was that the quantity of physiological data was stable. All trial data for each subject was averaged out and evaluated for steady state using the method highlighted in (Eq. 6 - 11). The steady state time average for each subject is shown in Fig. 7. Here the convergence of the rate of change of a running average of the summed EMG data is plotted against time. The data is stable in under 15 seconds for each subject. In addition, the max steady state time does not exceed 15 seconds for any trial of any subject. The data from all trials per subject were used to calculate this value.

The optimal controller (OP) was able to outperform all of the baseline conditions on average (Fig. 6). For the slow swing, OP reduced the muscle activity by 15.2% ($p < 1e\text{-}7$) compared to the no device condition. The OP was also able to outperform the zero torque condition by 19.7% ($p < 1e\text{-}4$). The OP of the slow controller was able to reduce muscle activity compared to the general controller as well by 14.5% ($p < 1e\text{-}4$). For the faster swing controller, the optimal was also able to significantly reduce the associated muscle activity for the no device and the zero torque conditions by 17.0% ($p < 1e\text{-}4$) and 23.6% ($p < 1e\text{-}4$) respectively. The optimal controller was also able to reduce the muscle activity in comparison to a fast swing general controller by 15.6% ($p = .0015$).

In terms of the Borg scale values, the optimal controller is perceived to lower effort compared to a majority of the baselines. This is concluded by observing the percent change of the mean Borg values between optimal and each baseline. The percent change for the Borg scale values calculated using Eq. 12 are reported in Table I.

TABLE I
Borg Value Comparison Against Baselines For Validation

Baseline	% change	
	Opt. Slow	Opt. Fast
No Device	-26.0%	-14.4%
Zero Assistance	-39.5%	-26.8%
General Control	-18.5%	4.9%

A preferred parameter set was found within the eight search iterations. An early stop condition where the parameters

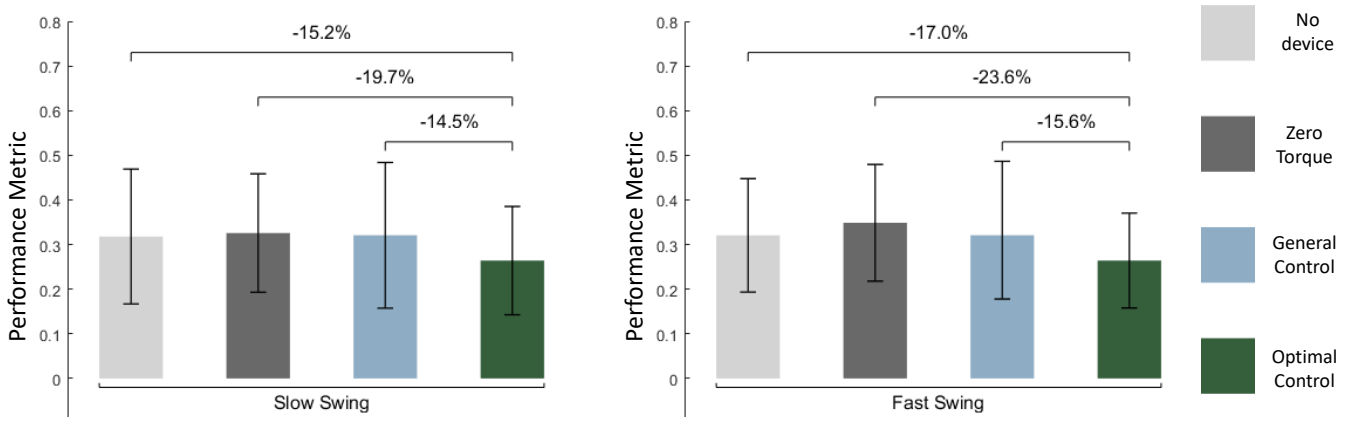

Fig. 6. Condition comparison results from the validation phase. The condition averages of the EMG performance metric are represented by the bar graph. The standard deviation is shown by whiskers. Percent changes between tests with three baseline conditions and tests with optimal control are shown above the horizontal brackets.

converge early is found for seven out of the eight subjects. The parameters of the eighth subject all converge except for one. The Lb parameter did not meet early stopping criteria but three similar values are observed, providing a strong indication that it is preferred by the acquisition function. The average number of trials required to tune for the eight subjects was 9.5 with a standard deviation of 1.87.

IV. Discussion

The optimization process demonstrates a well-performing ability to tune quickly and effectively, resulting in a noteworthy reduction of muscle activity compared to all baselines. In particular, the results establish the advantage of an optimal controller over arbitrary assistance, heavily indicating that tuning is a necessity. The use of EMG data for tuning is validated by the effectiveness of the tuning process, positioning EMG as a rapid and effective alternative to metabolic cost. The study achieves four times faster tuning compared to metabolic cost-based approaches [18], showcasing a significant advancement. When compared with prior EMG HIL optimization studies [40], our approach stands out by achieving tuning in as little as 2.38 minutes with consistent controller performance. These contributions enhance the practicality and applicability of EMG-based optimization.

The Borg scale results serve to add a layer of validation to the need for the optimization process. The values in Table I show that the assistance from the optimal controller provided a noticeable aid while swinging. The values of percent change from the baseline show that most subjects not only preferred the optimal condition but that there was also a significant reduction in the perceived effort across the comparison against the baseline conditions. The only exception to this is noticed with the optimal controller versus the general controller of the fast swing frequency. In this condition, it was more difficult for subjects to notice a distinguishable difference. The mean reflects an overall preference for the general controller despite physiological data showing that the opposite was true. This may be due to the higher demand for energy from the faster swing pace being perceived as more readily mitigated with impulse-style assistance that the general controller provides. Overall, the Borg scale data helps solidify the evidence that the optimal controller is noticeably preferred as is suggested by EMG performance data.

In addition to being able to optimize properly, the convergence of the EMG signal within 15 seconds showcases that the signal is capable of being harvested very quickly. This process stabilizes the signals and improves their SNR significantly. This challenges the existing mentality towards EMG by demonstrating its usability, despite often being considered unreliable. The innovative data processing methods showcase the utility of EMG despite its inherent noise.

A. Limitations and Future direction

The study design has limitations, including reliance on a single physiological metric for validation and a limited subject pool. Although EMG performance criteria have improved, they still yield significant measurement variance. Future research should employ multiple physiological metrics for cross-validation and include a larger subject pool for better correlation analysis. Additionally, exploring more demanding activities like squatting or walking would enhance evaluation. Addressing significant acclimation challenges requires a prolonged study with a multi-day protocol to understand individualized effects.

V. Conclusion

The importance of this study lies in its ability to achieve extremely fast and effective control tuning and improved EMG processing for optimization. The findings indicate that EMG optimization is not only quick and effective but also worthy of further investigation. Despite limitations, the generalizability of the findings is evident. When the method is applied to other activities such as walking and squatting in future efforts, particular consideration will be placed on the factors of acclimation, and multi-physiological validation. The study advances our understanding of rapid EMG optimization, offering a promising direction for future research and practical applications in the development of exoskeleton controllers.

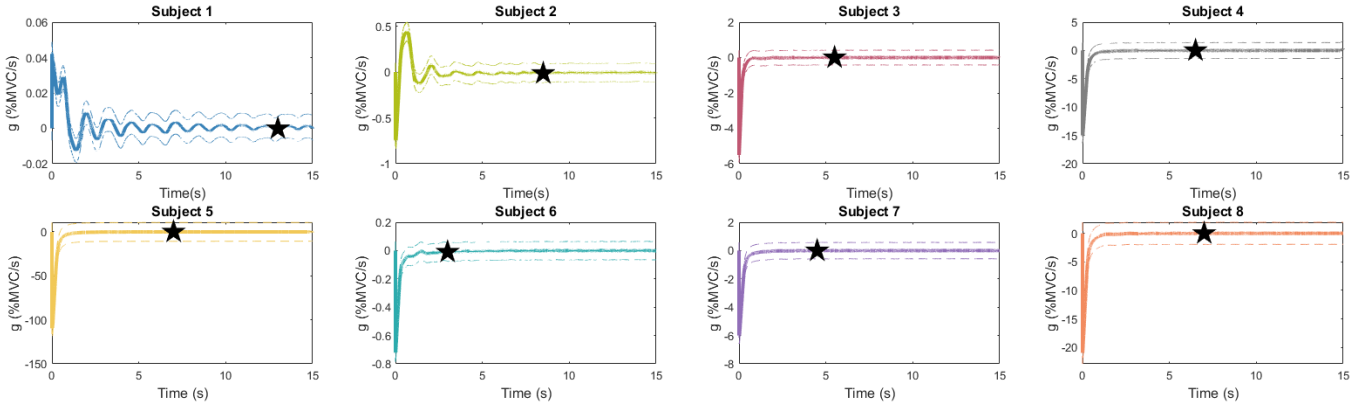

Fig. 7. The convergence data for each subject is represented as a bold average line with dotted lines showing the standard deviation. The variable g represents the sum of the derivative of the running average for the four sensors across all trials of a subject. The star indicates the time when a steady state is reached on average.

ACKNOWLEDGMENT

The authors would like to thank Subramanian Ramasay, and ChunMing Yang for volunteering as resident subjects for fine-tuning of the methods.

In addition, the authors would like to extend gratitude toward members of the Rehabilitation Robotics Laboratory at the University of Illinois at Chicago for their continued support and assistance.

REFERENCES

[1] Bing Chen et al. "State-of-the-art research in robotic hip exoskeletons: A general review". In: *Journal of Orthopaedic Translation* 20 (2020), pp. 4–13. ISSN: 2214-031X. DOI: https://doi.org/10.1016/j.jot.2019.09.006. URL: https://www.sciencedirect.com/science/article/pii/S2214031X19302104.

[2] Hong Han et al. "Selection of Muscle-Activity-Based Cost Function in Human-in-the-Loop Optimization of Multi-Gait Ankle Exoskeleton Assistance." eng. In: *IEEE transactions on neural systems and rehabilitation engineering : a publication of the IEEE Engineering in Medicine and Biology Society* 29 (2021). Place: United States, pp. 944–952. ISSN: 1558-0210 1534-4320. DOI: 10.1109/TNSRE.2021.3082198.

[3] E. Martini et al. "Lower-limb amputees can reduce the energy cost of walking when assisted by an Active Pelvis Orthosis". In: *2020 8th IEEE RAS/EMBS International Conference for Biomedical Robotics and Biomechatronics (BioRob)*. 2020, pp. 809–815. DOI: 10.1109/BioRob49111.2020.9224417.

[4] Philippe Malcolm et al. "A Simple Exoskeleton That Assists Plantarflexion Can Reduce the Metabolic Cost of Human Walking". In: *PLOS ONE* 8.2 (Feb. 2013). Publisher: Public Library of Science, pp. 1–7. DOI: 10.1371/journal.pone.0056137. URL: https://doi.org/10.1371/journal.pone.0056137.

[5] Luke M. Mooney, Elliott J. Rouse, and Hugh M. Herr. "Autonomous exoskeleton reduces metabolic cost of human walking during load carriage". In: *Journal of NeuroEngineering and Rehabilitation* 11.1 (May 2014), p. 80. ISSN: 1743-0003. DOI: 10.1186/1743-0003-11-80. URL: https://doi.org/10.1186/1743-0003-11-80.

[6] Steven H. Collins, M. Bruce Wiggin, and Gregory S. Sawicki. "Reducing the energy cost of human walking using an unpowered exoskeleton". In: *Nature* 522.7555 (June 2015), pp. 212–215. ISSN: 1476-4687. DOI: 10.1038/nature14288. URL: https://doi.org/10.1038/nature14288.

[7] Jeffrey R. Koller et al. "Learning to walk with an adaptive gain proportional myoelectric controller for a robotic ankle exoskeleton". In: *Journal of NeuroEngineering and Rehabilitation* 12.1 (Nov. 2015), p. 97. ISSN: 1743-0003. DOI: 10.1186/s12984-015-0086-5. URL: https://doi.org/10.1186/s12984-015-0086-5.

[8] Juanjuan Zhang et al. "Human-in-the-loop optimization of exoskeleton assistance during walking". In: *Science* 356.6344 (2017). _eprint: https://www.science.org/doi/pdf/10.1126/science.aal5054, pp. 1280–1284. DOI: 10.1126/science.aal5054. URL: https://www.science.org/doi/abs/10.1126/science.aal5054.

[9] Karl E. Zelik et al. "Systematic variation of prosthetic foot spring affects center-of-mass mechanics and metabolic cost during walking." eng. In: *IEEE transactions on neural systems and rehabilitation engineering : a publication of the IEEE Engineering in Medicine and Biology Society* 19.4 (Aug. 2011). Place: United States, pp. 411–419. ISSN: 1558-0210 1534-4320. DOI: 10.1109/TNSRE.2011.2159018.

[10] Rachel W. Jackson and Steven H. Collins. "An experimental comparison of the relative benefits of work and torque assistance in ankle exoskeletons." eng. In: *Journal of applied physiology (Bethesda, Md. : 1985)* 119.5 (Sept. 2015). Place: United States, pp. 541–557. ISSN:

1522-1601 0161-7567. DOI: 10.1152/japplphysiol.01133.2014.

[11] Roberto E. Quesada, Joshua M. Caputo, and Steven H. Collins. "Increasing ankle push-off work with a powered prosthesis does not necessarily reduce metabolic rate for transtibial amputees." eng. In: *Journal of biomechanics* 49.14 (Oct. 2016). Place: United States, pp. 3452–3459. ISSN: 1873-2380 0021-9290. DOI: 10.1016/j.jbiomech.2016.09.015.

[12] Matthew L. Handford and Manoj Srinivasan. "Robotic lower limb prosthesis design through simultaneous computer optimizations of human and prosthesis costs". In: *Scientific Reports* 6.1 (Feb. 2016), p. 19983. ISSN: 2045-2322. DOI: 10.1038/srep19983. URL: https://doi.org/10.1038/srep19983.

[13] Dominic James Farris, Benjamin D. Robertson, and Gregory S. Sawicki. "Elastic ankle exoskeletons reduce soleus muscle force but not work in human hopping." eng. In: *Journal of applied physiology (Bethesda, Md. : 1985)* 115.5 (Sept. 2013). Place: United States, pp. 579–585. ISSN: 1522-1601 0161-7567. DOI: 10.1152/japplphysiol.00253.2013.

[14] Daniel P. Ferris, Gregory S. Sawicki, and Monica A. Daley. "A PHYSIOLOGIST'S PERSPECTIVE ON ROBOTIC EXOSKELETONS FOR HUMAN LOCOMOTION." eng. In: *International journal of HR : humanoid robotics* 4.3 (Sept. 2007). Place: United States, pp. 507–528. ISSN: 0219-8436. DOI: 10.1142/S0219843607001138.

[15] D. Huang et al. "Global Optimization of Stochastic Black-Box Systems via Sequential Kriging Meta-Models". In: *Journal of Global Optimization* 34.3 (Mar. 2006), pp. 441–466. ISSN: 1573-2916. DOI: 10.1007/s10898-005-2454-3. URL: https://doi.org/10.1007/s10898-005-2454-3.

[16] Romy Lorenz et al. "The Automatic Neuroscientist: A framework for optimizing experimental design with closed-loop real-time fMRI". In: *NeuroImage* 129 (2016), pp. 320–334. ISSN: 1053-8119. DOI: https://doi.org/10.1016/j.neuroimage.2016.01.032. URL: https://www.sciencedirect.com/science/article/pii/S1053811916000380.

[17] Pengqing Ren et al. "Improving the Time Efficiency of sEMG-based Human-in-the-Loop Optimization". In: *2019 Chinese Control Conference (CCC)*. 2019, pp. 4626–4631. DOI: 10.23919/ChiCC.2019.8866157.

[18] Myunghee Kim et al. "Human-in-the-loop Bayesian optimization of wearable device parameters". In: *PLOS ONE* 12.9 (Sept. 2017). Publisher: Public Library of Science, pp. 1–15. DOI: 10.1371/journal.pone.0184054. URL: https://doi.org/10.1371/journal.pone.0184054.

[19] Daniel F. N. Gordon et al. "Human-in-the-Loop Optimization of Exoskeleton Assistance Via Online Simulation of Metabolic Cost". In: *IEEE Transactions on Robotics* 38.3 (2022), pp. 1410–1429. DOI: 10.1109/TRO.2021.3133137.

[20] Jessica C. Selinger and J. Maxwell Donelan. "Estimating instantaneous energetic cost during non-steady-state gait." eng. In: *Journal of applied physiology (Bethesda, Md. : 1985)* 117.11 (Dec. 2014). Place: United States, pp. 1406–1415. ISSN: 1522-1601 0161-7567. DOI: 10.1152/japplphysiol.00445.2014.

[21] Jessica C. Selinger and J. Maxwell Donelan. "Estimating instantaneous energetic cost during non-steady-state gait." eng. In: *Journal of applied physiology (Bethesda, Md. : 1985)* 117.11 (Dec. 2014). Place: United States, pp. 1406–1415. ISSN: 1522-1601 0161-7567. DOI: 10.1152/japplphysiol.00445.2014.

[22] Tamar R. Makin, Frederique de Vignemont, and A. Aldo Faisal. "Neurocognitive barriers to the embodiment of technology". In: *Nature Biomedical Engineering* 1.1 (Jan. 2017), p. 0014. ISSN: 2157-846X. DOI: 10.1038/s41551-016-0014. URL: https://doi.org/10.1038/s41551-016-0014.

[23] Keith E. Gordon and Daniel P. Ferris. "Learning to walk with a robotic ankle exoskeleton". In: *Journal of Biomechanics* 40.12 (2007), pp. 2636–2644. ISSN: 0021-9290. DOI: https://doi.org/10.1016/j.jbiomech.2006.12.006. URL: https://www.sciencedirect.com/science/article/pii/S0021929006004866.

[24] Jessica C. Selinger et al. "Humans Can Continuously Optimize Energetic Cost during Walking." eng. In: *Current biology : CB* 25.18 (Sept. 2015). Place: England, pp. 2452–2456. ISSN: 1879-0445 0960-9822. DOI: 10.1016/j.cub.2015.08.016.

[25] J. Rosen et al. "A myosignal-based powered exoskeleton system". In: *IEEE Transactions on Systems, Man, and Cybernetics - Part A: Systems and Humans* 31.3 (2001), pp. 210–222. DOI: 10.1109/3468.925661.

[26] Andrea Cimolato et al. "EMG-driven control in lower limb prostheses: a topic-based systematic review". In: *Journal of NeuroEngineering and Rehabilitation* 19.1 (May 2022), p. 43. ISSN: 1743-0003. DOI: 10.1186/s12984-022-01019-1. URL: https://doi.org/10.1186/s12984-022-01019-1.

[27] He Huang et al. "Continuous locomotion-mode identification for prosthetic legs based on neuromuscular-mechanical fusion." eng. In: *IEEE transactions on biomedical engineering* 58.10 (Oct. 2011). Place: United States, pp. 2867–2875. ISSN: 1558-2531 0018-9294. DOI: 10.1109/TBME.2011.2161671.

[28] Gabriel Aguirre-Ollinger. "Learning muscle activation patterns via nonlinear oscillators: Application to lower-limb assistance". In: *2013 IEEE/RSJ International Conference on Intelligent Robots and Systems*. 2013, pp. 1182–1189. DOI: 10.1109/IROS.2013.6696500.

[29] D. A. Winter and H. J. Yack. "EMG profiles during normal human walking: stride-to-stride and inter-subject variability." eng. In: *Electroencephalography and clinical neurophysiology* 67.5 (Nov. 1987). Place: Ireland, pp. 402–411. ISSN: 0013-4694. DOI: 10.1016/0013-4694(87)90003-4.

[30] C. Fleischer, C. Reinicke, and G. Hommel. "Predicting the intended motion with EMG signals for an exoskeleton orthosis controller". In: *2005 IEEE/RSJ International Conference on Intelligent Robots and Systems*.

2005, pp. 2029–2034. DOI: 10.1109/IROS.2005.1545504.

[31] Daniel F. N. Gordon et al. “Bayesian Optimisation of Exoskeleton Design Parameters”. In: *2018 7th IEEE International Conference on Biomedical Robotics and Biomechatronics (Biorob)*. 2018, pp. 653–658. DOI: 10.1109/BIOROB.2018.8487720.

[32] Matthew B. Yandell et al. “Physical interface dynamics alter how robotic exosuits augment human movement: implications for optimizing wearable assistive devices”. In: *Journal of NeuroEngineering and Rehabilitation* 14.1 (May 2017), p. 40. ISSN: 1743-0003. DOI: 10.1186/s12984-017-0247-9. URL: https://doi.org/10.1186/s12984-017-0247-9.

[33] Canjun Yang et al. “Current developments of robotic hip exoskeleton toward sensing, decision, and actuation: A review”. In: *Wearable Technologies* 3 (2022). Publisher: Cambridge University Press, e15. DOI: 10.1017/wtc.2022.11.

[34] Eric Brochu, Vlad M. Cora, and Nando de Freitas. “A Tutorial on Bayesian Optimization of Expensive Cost Functions, with Application to Active User Modeling and Hierarchical Reinforcement Learning”. In: *CoRR* abs/1012.2599 (2010). arXiv: 1012.2599. URL: http://arxiv.org/abs/1012.2599.

[35] *Optimal Swing Assistance Using a Hip Exoskeleton: Comparing Simulations With Hardware Implementation*. Vol. Volume 8: 47th Mechanisms and Robotics Conference (MR). International Design Engineering Technical Conferences and Computers and Information in Engineering Conference. Aug. 2023, V008T08A074. DOI: 10.1115/DETC2023-117126. eprint: https://asmedigitalcollection.asme.org/IDETC-CIE/proceedings-pdf/IDETC-CIE2023/87363/V008T08A074/7061940/v008t08a074-detc2023-117126.pdf. URL: https://doi.org/10.1115/DETC2023-117126.

[36] SENIAM - Surface EMG for Non-Invasive Assessment of Muscles. *SENIAM: Surface EMG for Non-Invasive Assessment of Muscles*. Accessed on Date. Date of access. URL: http://seniam.org/sensor_location.htm.

[37] Hiroshi Akima. “A New Method of Interpolation and Smooth Curve Fitting Based on Local Procedures”. In: *J. ACM* 17.4 (Oct. 1970), pp. 589–602. ISSN: 0004-5411. DOI: 10.1145/321607.321609. URL: https://doi.org/10.1145/321607.321609.

[38] Marcin Straczkiewicz, Emily J. Huang, and Jukka-Pekka Onnela. “A “one-size-fits-most” walking recognition method for smartphones, smartwatches, and wearable accelerometers”. In: *npj Digital Medicine* 6.1 (Feb. 23, 2023), p. 29. ISSN: 2398-6352. DOI: 10.1038/s41746-022-00745-z. URL: https://doi.org/10.1038/s41746-022-00745-z.

[39] Prabhaker Mishra et al. “Descriptive statistics and normality tests for statistical data.” In: *Annals of cardiac anaesthesia* 22.1 (Mar. 2019). Place: India, pp. 67–72. ISSN: 0974-5181 0971-9784. DOI: 10.4103/aca.ACA_157_18.

[40] Liang Ma et al. “EMG-based Human-in-the-loop Optimization of Ankle Plantar-flexion Assistance with a Soft Exoskeleton”. In: *2022 International Conference on Advanced Robotics and Mechatronics (ICARM)*. 2022, pp. 453–458. DOI: 10.1109/ICARM54641.2022.9959677.